Dual-path glucose electrooxidation reaction on Ni(OH)2/NiOOH catalysts in alkaline media

Alejandra Medrano-Banda, Julie Guehl, Gwénaëlle Kéranguéven, Alexandr Oshchepkov, Elena Savinova, Pierre-Antoine Bonnefont

Dual-path Glucose Electrooxidation Reaction on $Ni(OH)_2$/NiOOH Catalysts in Alkaline Media

Alejandra Medrano-Banda[1], Julie Guehl[1], Gwénaëlle Kéranguéven, Alexandr Oshchepkov[1], Elena Savinova[1], Antoine Bonnefont[2]

[1]*Institut de Chimie et Procédés pour l'Energie, l'Environnement et la Santé, UMR 7515 CNRS-University of Strasbourg; 25 rue Becquerel 67087 Strasbourg Cedex, France*
[2]*Univ. Grenoble Alpes, Univ. Savoie Mont Blanc, CNRS, Grenoble INP (Institute of Engineering and Management), LEPMI, 38000 Grenoble, France*

Abstract

Glucose electrooxidation has been widely studied for its application in biosensors, fuel cells and electrosynthesis of value-added products. Nickel is known to catalyze the glucose oxidation reaction (GOR) in alkaline media, but the mechanism, the nature of the active sites, and reaction products are still being debated. This study focuses on elucidating the reaction pathways of the GOR on a $Ni(OH)_2$/NiOOH electrode through electrochemical measurements, *in-situ* Fourier transform infrared spectroscopy (FTIRS) and microkinetic modeling. The electrode was prepared by Ni electrodeposition on glassy carbon (Ni_{ED}/GC) followed by electrochemical oxidation into $Ni(OH)_2$/NiOOH. The shape of the cyclic voltammograms obtained during the GOR was found to be significantly influenced by the presence of Fe impurities in the NaOH electrolyte. With the help of microkinetic modeling, a dual-path mechanism was proposed for the glucose electrooxidation on the $Ni(OH)_2$/NiOOH surface, comprised of Eley-Rideal and Langmuir-Hinshelwood pathways, with NiOOH reacting either with glucose from solution or adsorbed on $Ni(OH)_2$ sites. *In-situ* FTIR measurements reveal the formation of formate at potentials as low as 1.17 V vs. RHE.

Keywords

Glucose oxidation reaction (GOR); Nickel hydroxide; Iron; *In situ* Fourier Transform Infrared Spectroscopy (FTIR); Meanfield kinetic modeling

Highlights

- GOR in alkaline media is catalyzed by the $Ni(OH)_2$/NiOOH transition but not the Ni/$Ni(OH)_2$ one
- Presence of Fe impurities impacts the GOR on $Ni(OH)_2$/NiOOH electrodes
- *In-situ* FTIRS confirms formate as one of the main products of the GOR on Ni
- Microkinetic modeling suggests that GOR on Ni occurs through a dual-path mechanism

1. Introduction

The increasing demand of pharmaceutical, food, and energy industry has sparked interest in the catalytic conversion of biomass to fuels and valuable chemicals as an alternative to mitigate global warming and promote a carbon-neutral energy cycle [1,2]. Glucose, being one of the most abundant monosaccharides,

has become a protagonist in biomass transformation; more specifically, glucose electrooxidation has been widely studied for its application in biosensors, electrolysis for H_2 production and electrosynthesis of value-added products [3]. One of the biggest challenges when studying the glucose oxidation reaction (GOR) is that it can proceed through several oxidation steps, which can lead to multiple products [4], therefore the use of electrocatalysts that are inexpensive, efficient, and selective becomes crucial. Noble metals, such as Au [5], Pt [6] and Pd [7] have been used to efficiently catalyze the GOR in alkaline media. Oxides of transition metal, such as Co [8], Cu [9] and Ni [10,11] are promising non-precious alternative to noble metals, and have indeed proven to catalyze the glucose oxidation in alkaline media, albeit at higher potential. In particular, nickel has been extensively studied for oxidation of glucose and many other organic molecules, but the corresponding reaction mechanisms are still poorly understood [12–14].

It is well known that the nickel surface state depends on the applied electrode potential and undergoes a consecutive transformation from metallic to a hydrated α-$Ni(OH)_2$, an anhydrous β-$Ni(OH)_2$, and then a NiOOH phase (for further details see Section 3.1). Most of the GOR studies focus on the high potential region with the reaction being catalyzed through the electrochemical oxidation of β-$Ni(OH)_2$ into NiOOH (Eq. 1). In the 1960's Fleischmann *et al.* [15] were one of the first to study the oxidation of organic molecules, including glucose, on Ni electrodes, and they proposed the following mechanism:

$$Ni(OH)_2 + OH^- \rightleftarrows NiOOH + H_2O + e^- \quad (1)$$

$$NiOOH + \text{glucose} \rightarrow Ni(OH)_2 + \text{intermediate} \quad (2)$$

$$NiOOH + \text{intermediate} \rightarrow \text{product} + Ni(OH)_2 \quad (3)$$

Here the $Ni(OH)_2$ oxide species are first electrochemically oxidized to form NiOOH (Eq. 1), and later react with glucose in a series of two chemical steps (Eq. 2 and 3). This mechanism is known as an electrochemical (Eq. 1) - chemical (Eq. 2) catalytic mechanism (EC') [16], because the $Ni(OH)_2$ species is regenerated within the catalytic cycle. At high potential, when the chemical step becomes the rate-determining reaction step, the cyclic voltammogram (CV) of this EC' mechanism is expected to exhibit a current plateau [17]. Even though the EC' mechanism has been widely referenced in the literature, later works have suggested that there might be more steps in the GOR mechanism. For example, Danaee *et al.*, showed that the electrochemical impedance spectra measured during the GOR on Ni exhibit a negative differential resistance [18–20] which cannot be explained within Fleischmann's mechanism [15]. To account for the experimental observations, Danaee *et al.* proposed that glucose adsorbs on the NiOOH sites [20]. In this context, it is also worth noting that recently Bender *et al.* [21], when studying the oxidation of various alcohols and aldehydes on NiOOH with electrochemical and computational methods, suggested that the reaction could follow two pathways: (i) through deprotonation of the catalyst and (ii) hydride transfer from

organic molecule to the catalyst surface. Thus, so far there is no consensus either regarding the mechanism of the glucose (and other organic molecule) oxidation or the nature of active sites (NiOOH vs. $Ni(OH)_2$) on Ni.

Moreover, the products of the GOR on Ni are still poorly understood. Toghill *et al.* and Zhao *et al.*, have argued that the oxidation of glucose occurs in a $2e^-$ reaction to form gluconolactone as an intermediate, which later transforms to gluconate as the final product [22,23]. However, to the best of our knowledge, this has not been confirmed by any analytical or spectroscopy techniques.

Furthermore, all the previous mechanistic studies of the GOR on Ni neglected the potential impact of iron impurities in alkaline electrolytes, the latter known to significantly lower the overpotential for the oxygen evolution reaction (OER) and provoke an anodic shift in the $Ni(OH)_2$/NiOOH redox peak potential [24, 25]. Considering that commercial alkalis contain between 36 ppb and 1 ppm of Fe (depending on the degree of purity) [26], it can be assumed that the previous studies of the GOR might have suffered from a non-negligible contribution of the OER to the total current, the latter affecting interpretation of the GOR. Xiang *et al.* studied the GOR on $Ni(OH)_2$-modified Au electrodes with electrochemical quartz crystal impedance and argued that a decrease of the current in the potential interval from 1.56 to 1.65 V *vs.* RHE could either be due to a decrease of the glucose coverage or to a competition of the GOR and OER for the surface sites [27].

Since nearly all previous efforts were likely carried out using Fe-contaminated alkaline electrolytes, it is not clear if the unintentional Fe incorporation in $Ni(OH)_2$/NiOOH affects the mechanism and activity of Ni in the GOR in the high potential region. Furthermore, it is now well established that the electrocatalytic activity of Ni electrodes between -0.4 and 0.4 V vs RHE strongly depends on their surface state which can be either fully metallic, partially oxidized or passivated depending on the electrode's history [28] and it was not clear if the GOR might occur at low overpotentials on fully metallic or partially oxidized Ni surface.

In this contribution, we study the GOR on Ni electrodeposited on GC (Ni_{ED}/GC) in commercial and Fe-purified NaOH by employing electrochemistry, *in situ* FTIRS and microkinetic modeling with the objectives to (i) determine potential of the GOR "onset", (ii) elucidate main GOR pathways in the absence of Fe^{3+} impurities in alkaline electrolyte, and (iii) determine the products of the GOR on Ni. These studies revealed that the GOR on Ni does not occur below ~1.2 V vs. RHE. They further showed that the presence of Fe impurities in NaOH increases the parasitic contribution of the OER and also affects the shape of the GOR current-potential curve. By confronting the experimental current-potential curves to the results of microkinetic modeling we conclude that the GOR proceeds on the $Ni(OH)_2$/NiOOH active sites via a dual-

path mechanism involving an Eley-Rideal (ER) and a Langmuir-Hinshelwood (LH) pathways. Finally, formation of a carboxylate product of the GOR could be corroborated through *in situ* FTIRS.

2. Experimental

2.1. Chemicals

Solutions were prepared using ultra-pure water with the resistivity of 18.2 MΩ·cm and TOC < 1 ppb (PURELAB Chorus 1). The reagents $NiSO_4 \cdot 6H_2O$ (99.99 %, Aldrich), $(NH_4)_2SO_4$ (99.0 %, Aldrich), $(NH_4)_2Cl$ (99.999 % metal basis, Alfa Aesar), HCl (37 %, ChemLab), glucose (ACS reagent, Aldrich) and sodium gluconate (ACS reagent, Aldrich) were used as received. NaOH (50 % in water, Aldrich) was used either as-received (Fe^{3+} concentration is expected to be around 9±1 ppb for 0.1 M solution [29,30]) or after Fe-purification carried out according to the protocol inspired by Trotochaud et al. [31] and specified in Supplementary Information (S.1).

2.2. Ni electrodeposition on Glassy Carbon

Ni_{ED}/GC samples were prepared by Ni electrodeposition on a 5 mm diameter glassy carbon (GC) electrode that was polished with Al_2O_3 powder of 1 and 0.3 μm particle diameter for 5 minutes each and then sonicated in acetone, ethanol and deionized water to remove any remaining polishing residues (10 minutes in each solvent). Electrodeposition of Ni on a GC surface was performed at 25°C from the N_2-saturated 0.01 M $NiSO_4$ and 0.1 M $(NH_4)_2SO_4$ solution in a glass cell with separate compartments for working (GC disk), counter (Ni wire), and reference (a $Hg|Hg_2SO_4|K_2SO_4$ (sat.) electrode, MSE) electrodes using a double-step (E_1 = -1.5 and E_2 = -1.25 V *vs*. MSE for 120 and 400 s, respectively) potentiostatic regime with rotation at 400 rpm. Immediately after the deposition, the electrode was washed and quickly transferred into the Teflon cell with alkaline electrolyte for further electrochemical measurements.

2.3. Electrochemical measurements

All electrochemical measurements were performed in a three-electrode Teflon cell at 25°C in either Fe-purified or unpurified 0.1 M NaOH electrolyte with Ni_{ED}/GC as working electrode, Pt wire as counter electrode and Hg|HgO|0.1 M NaOH (E = 0.94 V vs. RHE) as reference electrode. Unless otherwise stated experiments were performed without rotation. First CVs were measured in the -0.2 to 0.4 V vs. RHE potential region at 20 $mV \cdot s^{-1}$ and the charge of the anodic peak was used to determine the electrochemical surface area (ECSA) of the electrodes by using the constant 514 $\mu C \cdot cm^{-2}$ (corresponding a monolayer α-$Ni(OH)_2$ formation [32]). The electrochemical surface area (ECSA) was estimated as 0.93 cm^2, and the roughness factor of the electrode estimated as the ratio of the ECSA to the geometric surface area (0.197 cm^2) was found to be approximately 4.5. Afterward, the growth of a $Ni(OH)_2$/NiOOH layer was achieved by applying a 1.55 V *vs.* RHE for 20 minutes. To study the GOR, CVs were measured from 0.93 to 1.6 V vs. RHE at 20 $mV \cdot s^{-1}$ in the presence and absence of glucose in the solution. Glucose was dissolved in 0.1

M NaOH to obtain the solution with 0.5 M concentration, which then was added to the electrochemical cell in a step-wise manner to reach the target concentration.

2.4. FTIRS measurements

Spectrochemical measurements were performed at room temperature with a Bruker Vertex 80v Brucker Fourier transform infrared spectrometer equipped with a MCT detector (N_2-liquid temperature) using a ZnSe prism. The GOR on Ni disk (⌀ = 1 cm) was performed in a N_2 saturated unpurified 0.1 M NaOH solution using a glass cell with Pt wire as counter electrode and a Hg|HgO in 0.1 M NaOH (E = 0.94 V vs. RHE) reference electrode. The spectra were collected in a double-sided acquisition mode between wavenumbers from 4000 to 700 cm^{-1} with a resolution of 1 cm^{-1}. In order to obtain a single-beam spectrum, 64 interferograms were co-added and then Fourier transformed. The protocol of potentiostatic measurements was inspired by the work of Oshchepkov *et al.* [33] and consists of the following steps: (*i*) the Ni disk electrode was submitted to 1.55 V *vs.* RHE for 30 minutes to grow $Ni(OH)_2$/NiOOH surface layer until the stabilization of current when cycling in the 0.93 to 1.60 V vs. RHE region, subsequently (*ii*) glucose was injected to the cell (achieving the final concentration of 5 mM) and a CV was recorded in the same potential interval, then (*iii*) the potential equal to 1 V *vs.* RHE was applied to the working electrode, at which it was pressed to the prism and a background spectrum was recorded, finally *(iv*) the electrode was polarized at the potential of interest (E = 1.17 to 1.57 V vs RHE) at which a series of FTIR spectra (typically 8) was collected in order to see the dynamics of their evolution with time.

All spectra of the reference compounds (glucose, gluconate, formate) were recorded in ATR configuration using a hemispherical ZnSe prism and 64 interferograms with 1 cm^{-1} resolution.

2.5. Ni_{ED}/GC electrode characterization

2.5.1. Scanning electron microscopy

The morphology of Ni electrodeposited on GC was studied by Scanning Electron Microscopy (SEM) using a Zeiss Gemini SEM500 microscope at 1 kV voltage.

2.5.2. Inductively Coupled Plasma Mass Spectroscopy

Determination of the mass of Ni in the Ni_{ED}/GC samples and estimation of the Faradaic efficiency of the electrodeposition were based on the inductively coupled plasma mass spectrometry (ICP-MS) measurements performed using a Varian 720 spectrometer. The sample probe was obtained by electrodissolution of the catalyst layer from the top surface of the GC cylinder (protocol adapted from [34]). For this a freshly prepared electrode was immersed in a 5 mL three-electrode electrochemical cell containing 0.5 M NH_4Cl + 0.01 M HCl at the potential of -0.04 V vs. RHE, followed by recording the anodic dissolution profile at 1 $mV \cdot s^{-1}$ and 400 rpm. Saturated calomel electrode (SCE, E_{SCE} = 0.362 V *vs*

RHE) and Pt wire were employed as the reference and counter electrodes, respectively. The electrolyte used was transferred to a glass vial with a known mass to avoid mistakes caused by evaporation. The MS was calibrated using standards (1000 $mg \cdot L^{-1}$, CPI).

2.6. Kinetic model of glucose oxidation reaction on Ni

A mean-field microkinetic model of the GOR on Ni includes the $Ni(OH)_2$ to NiOOH transition (Eq. 1) approximated with a Langmuir isotherm model, in which the $Ni(OH)_2$ and the NiOOH are treated as surface species for simplicity. The model also includes adsorption/desorption of glucose on $Ni(OH)_2$ sites (also described by Langmuir isotherm) and reaction of the adsorbed glucose, adsorbed intermediate species and glucose in solution with NiOOH species. Charge-transfer steps are assumed to obey Butler-Volmer equations. Further modeling details are specified in the "Results and discussion" section and in supplementary information (S.4).

3. Results and discussion

3.1. Ni_{ED}/GC electrode characterization

A SEM micrograph of a fresh Ni_{ED}/GC electrode prepared through double-potential step deposition (Figure S1) is presented in Figure 1a, and shows a porous Ni film composed of agglomerated particles with a diameter of around 120 nm. The morphology of the deposits can be explained by continuous nucleation (on both GC and Ni sites) and growth of Ni particles as well as the occurrence of the hydrogen evolution reaction (HER) on their surface during the deposition. Examination of a Ni_{ED}/GC sample exposed to potential cycling in the presence of glucose did not reveal any noticeable morphology changes (Figure S2).

During the electrodeposition, the reduction of Ni is in competition with the HER and therefore the overall charge passed comprises contributions of both reactions. The amount of Ni deposited on GC was determined by dissolving electrodeposited Ni, and then quantifying Ni^{2+} by ICP-MS, which resulted in ~14 µg of Ni on a GC disk of 0.195 cm^2. This corresponds to a Faradaic efficiency of Ni deposition of 63%.

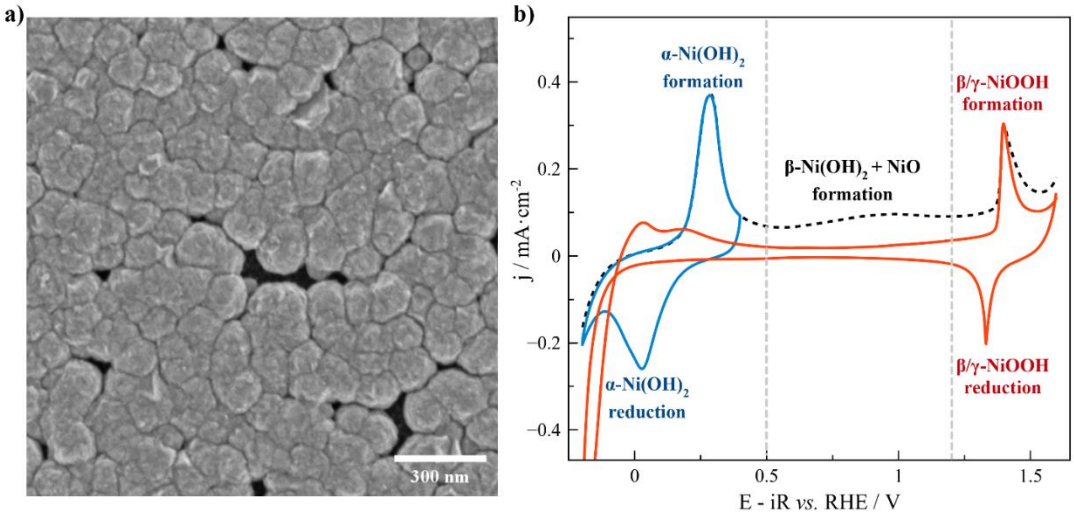

Figure 1. a) SEM image of Ni electrodeposited on GC, and b) Cyclic voltammetry of the Ni_{ED}/GC electrode in purified 0.1 M NaOH at 25°C and v = 20 mV·s^{-1} (The ECSA of Ni was estimated as 0.93 cm^2, see Experimental). Currents are normalized to the geometric surface area. The first blue CV covers the potential range from -0.2 to 0.4 V vs. RHE, while the dashed black and red CVs (first scan and second scan respectively) cover the potential range from -0.3 to 1.6 V vs. RHE. The figure is inspired from the paper [28].

3.2. Electrochemical measurements on freshly prepared Ni_{ED}/GC

Figure 1b shows CVs of Ni_{ED}/GC obtained in Fe-purified 0.1 M NaOH. In the potential interval from -0.1 to 0.4 V vs. RHE one may observe reversible oxidation of metallic Ni to surface α-$Ni(OH)_2$, the latter being known to comprise of $Ni(OH)_2$ layers with H_2O molecules and ions incorporated in between [35]. Above 0.4 V and up to 1.2 V vs. RHE, the α-$Ni(OH)_2$ is known to be converted into a more stable β-$Ni(OH)_2$ structure, which in contrast to α-$Ni(OH)_2$ cannot be electrochemically reduced to metallic Ni at 0 V vs. RHE [28]. Finally, in the 1.2 to 1.6 V vs. RHE potential region, α-/β-$Ni(OH)_2$ species undergo further transformation into γ-/β-NiOOH, which manifests itself by a pair of anodic and cathodic peaks around 1.35 V vs. RHE [36]. It is important to point out that a partially oxidized Ni electrode comprised of both metallic and oxidized Ni exhibits a significantly higher activity in the hydrogen evolution and oxidation reactions (see red curve in Figure 1b), which was attributed to a decrease of the strength of the hydrogen (H_{ad}) adsorption compared to metallic Ni [37].

The GOR was studied first in the low potential region where the formation of α-$Ni(OH)_2$ at the surface is observed. However, no difference either in the current amplitude or CV shape was observed in the presence and in the absence of glucose (Figure S3), which indicates that the GOR does not proceed in this potential region. For this reason, further studies of glucose oxidation were focused on the potential interval from 0.93 to 1.6 V vs. RHE.

The influence of Fe impurities was explored by comparing CVs of Ni_{ED}/GC in as-received commercial and Fe-purified NaOH electrolyte (Figure 2). In glucose-free electrolyte (black curve) the OER 'onset' potential is around 1.55 V vs. RHE in unpurified electrolyte, while in Fe-purified electrolyte no OER current is observed up to 1.6 V vs. RHE. The shift of the OER 'onset ' in the presence of Fe is in agreement with the literature and was attributed to Fe incorporation into the NiOOH structure, resulting in the formation of a more OER-active $Ni_xFe_{1-x}(OH)_2$ [38]. In the presence of glucose, the CVs in Fe-purified and unpurified electrolyte show noticeable differences (Figure 2). For glucose concentrations above 2 mM, the GOR current significantly decreases after reaching a maximum at approximately 1.45 V vs. RHE, and this decrease is more pronounced in Fe-purified electrolyte, which may be attributed to the 'delayed' OER. Also, in Fe-purified electrolyte, only one GOR peak is observed in the anodic scan, while two anodic peaks (at 1.45 and 1.50 V vs. RHE) are clearly seen in Fe-contaminated solutions. The current 'plateau', reported in previous studies of the GOR on Ni electrodes between 1.45 to 1.60 V vs. RHE [39–41], was observed only for glucose concentrations below 1 mM. Furthermore, when comparing the CVs in the presence and in the absence of Fe impurities at different glucose concentrations (Figure S4), it is possible to observe a slight displacement of the GOR 'onset' to positive potentials in the unpurified electrolyte, the latter could be attributed to the Fe incorporation in the $Ni(OH)_2$/NiOOH structure [42] and phase transformations (α-$Ni(OH)_2$/γ-NiOOH into β-$Ni(OH)_2$/β-NiOOH [31]), which are known to be dependent on the Fe impurities. Indeed, the hydrated α-$Ni(OH)_2$/γ-NiOOH phases are supposedly favored in the presence of Fe [43], which could be yet another reason for slightly different catalytic behavior in purified and unpurified NaOH. Another difference is the higher GOR current plateau observed in the potential interval between 1.45 and 1.55 V vs. RHE at low glucose concentrations in the presence of iron impurities (see Fig. S4, the CVs at 0.1, 0.5 and 1 mM glucose concentrations).

Except for the aforementioned, the electrochemical behavior of Ni_{ED}/GC in the presence of glucose shows common trends between Fe-purified and unpurified electrolytes. In both electrolytes the 'onset' potential is around 1.2 V vs. RHE (~0.1 V before the onset of the $Ni(OH)_2$/NiOOH peak), the anodic peak (albeit of different shape) is observed both in the positive and in the negative potential scan, and the anodic GOR current increases linearly with the concentration in the studied concentration range. For the sake of avoiding the contribution of the parasitic OER and in order to have a better understanding of the GOR, the rest of the discussion will be focused on the Fe-purified electrolyte (Figure 2b).

Additionally, because the GOR on Ni is expected to follow an EC' mechanism, measurements of current-potential curves at different potential scan rates were performed in the absence and in the presence of 1 mM glucose in 0.1 M NaOH solution (Figure S6), to provide further information on the relative kinetics of the $Ni(OH)_2$/NiOOH redox transition and of the GOR. At fast potential scan rates (i.e. above 500 $mV \cdot s^{-1}$) the

CVs in the presence and in the absence of glucose are identical, suggesting that they are fully dominated by the $Ni(OH)_2$/NiOOH redox transition, the kinetics of the glucose oxidation being too slow to affect the CV shape. As the scan rate is decreased, a "symmetric" CV of the $Ni(OH)_2$/NiOOH transition exhibiting positive currents in the anodic scan and negative currents in the cathodic one, gradually transforms in an "asymmetric" CV resulting from an interplay of fast $Ni(OH)_2$/NiOOH transition and a slow GOR. These measurements agree with previously reported scan rate dependence studies of Danaee *et al.* and Yi *et al.* for the GOR on Ni electrodeposited on either GC [20] or Ti [40].

Finally, the start of the GOR at a potential substantially lower than the 'onset' of the $Ni(OH)_2$/NiOOH transition does not agree with the mechanisms proposed either by Fleischmann *et al*. or Danaee *et al* [15, 19]. The drop of current after reaching a maximum is not in agreement with Fleischmann's model either, the latter predicting a current plateau at high overpotential. To confirm that the current peak on Ni_{ED}/GC electrodes is the reaction- rather than mass transport-controlled, experiments were performed at various rotation rates in the presence of 3 mM glucose (Figure S5). Even though the cyclic voltammograms showed a small increase in current with the rotation rate, no diffusion-limited plateau could be observed. All of the above question the validity of the highly cited Fleischmann's *et al.* The drop of current after reaching a maximum is not in agreement with Fleischmann's model either, the latter predicting a current plateau at high overpotential. To confirm that the current peak on Ni_{ED}/GC electrodes is the reaction- rather than mass transport-controlled, experiments were performed at various rotation rates in the presence of 3 mM glucose (Figure S5). Even though the cyclic voltammograms showed a small increase of current with the rotation rate, no diffusion-limited plateau could be observed [15] model of the GOR on Ni. To further advance our understanding of the latter, we performed microkinetic modeling.

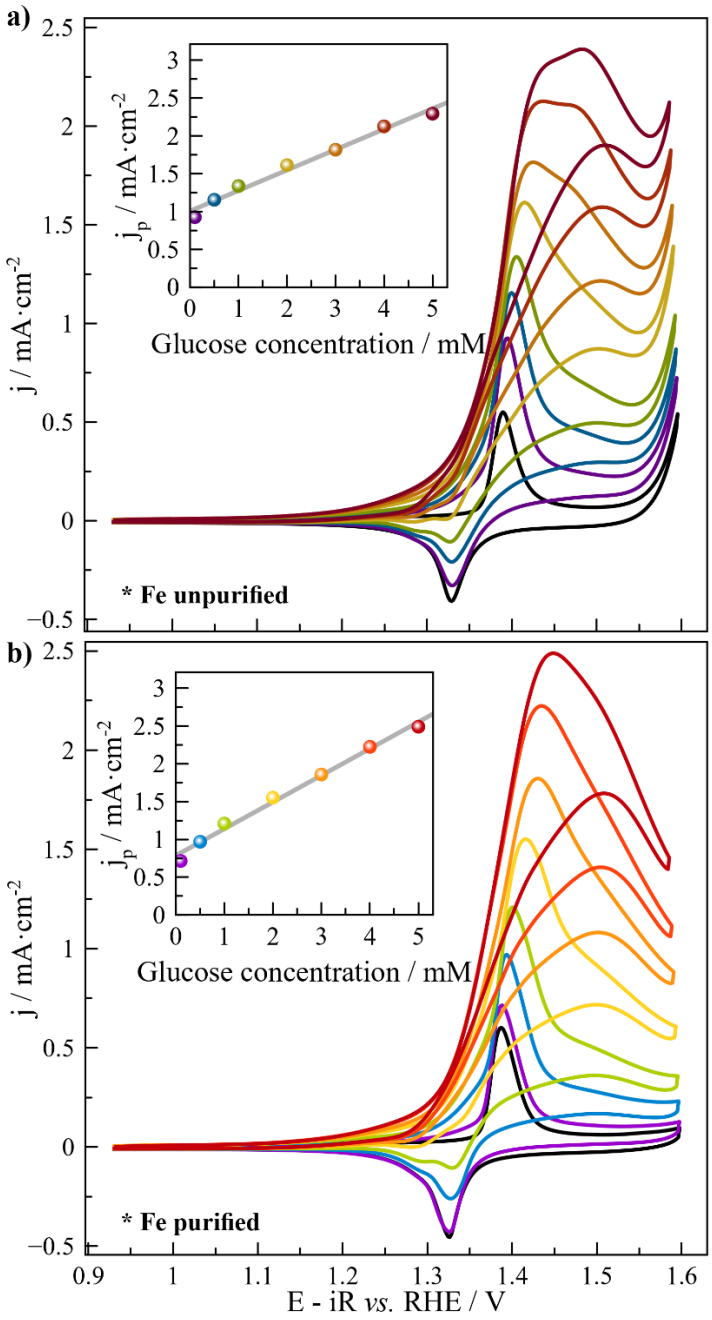

Figure 2. Cyclic voltammograms of the Ni_{ED}/GC electrode in a) Fe unpurified and b) Fe purified 0.1 M NaOH solution in the absence and presence of 0.1, 0.5, 1, 2, 3, 4 and 5 mM glucose in the solution at v = 20 mV·s^{-1} and 25ºC; insets show the dependency of the anodic peak current on the concentration of glucose in the solution. Currents are normalized to the geometric surface area.

3.3. Kinetic model of glucose oxidation reaction on Ni

Microkinetic modeling was applied to rationalize the influence of the glucose concentration and scan rate on the overall shape of the GOR current-potential curves, and this way to elucidate main GOR pathways

and provide a rough estimation of the main reaction rate constant values involved in the GOR. To achieve this the $Ni(OH)_2$/NiOOH redox transformation in the absence of glucose in solution was first modeled (Eq. 1). In a first approximation, it was assumed that this transition occurs only at the electrode surface and obeys Langmuir isotherm, thus neglecting that the NiOOH follows a 3D growth model [44]. The standard surface redox potential $E°_1$ and the charge transfer kinetic constant k_1 were adjusted to reproduce the potential of the experimentally observed redox peaks. In Figure 3 one may observe the computed CV of Ni in the absence of glucose (black curve), where the potential of the redox peaks is in good agreement with the experimental data, however, the peaks are broader than in the experiment. Note that Frumkin isotherm [45] with attractive adsorbate interactions allows to better reproduce the sharpness of the $Ni(OH)_2$/NiOOH redox peaks, but not necessarily their symmetrical shape (Figure S7). Nevertheless, in what follows the modeling was performed within a simple Langmuir model which allows only a semi-quantitative agreement between the simulations and experimental data.

The first model applied to describe the GOR on Ni was inspired by the Fleischmann *et al.* [15], model of oxidation of organic molecules on Ni in alkaline media (Eqs. 2 to 3) with the only exception that an intermediate (likely a radical) is considered to be adsorbed on the electrode surface (Eqs. 2' to 3'):

$$NiOOH_{ads} + \text{glucose} \rightarrow Ni(OH)_2\text{–intermediate}_{ads} \quad (2')$$

$$Ni(OH)_2\text{–intermediate}_{ads} + NiOOH \rightarrow \text{product} + 2Ni(OH)_2 \quad (3')$$

Since in this model glucose from solution reacts with NiOOH at the surface, in what follows we will name the corresponding mechanism Eley-Rideal [46]. The rates of formation of the $NiOOH_{ads}$, the adsorbed intermediate and the product, as well as corresponding differential equations for the adsorbate coverages are specified in Supporting Information (S.4.2). The total faradaic current density, assuming Langmuir model and Butler-Volmer kinetics for the charge transfer process, is given by Eq. 4:

$$j_F = FS_t\left(k_1 \exp\left(\frac{\alpha F(E-E_1^\circ)}{RT}\right)(1-\theta_{NiOOH}-2\theta_{int})-k_1\theta_{NiOOH}\exp\left(-\frac{(1-\alpha)F(E-E_1^\circ)}{RT}\right)\right) \quad (4)$$

Where S_t is the mole number of active Ni sites per electrode geometric surface area, k_1 corresponds to the rate constant of Eq. 1, E_1° is the $Ni(OH)_2$/NiOOH standard potential, and θ_{int} and θ_{NiOOH} are the surface coverages of the intermediate and NiOOH species, respectively. The simulations assumed fast reaction kinetics between the adsorbed intermediate species and NiOOH (large k_3) in order to avoid blocking (or poisoning) of the surface with the adsorbed intermediate, which may be observed for small values of k_3, as displayed in Figure S8.

CVs computed within the ER mechanism are shown in Figure 3a. As expected, the GOR 'onset' coincides with the $Ni(OH)_2$/NiOOH 'onset', and at high potential, they exhibit a current plateau proportional to the glucose concentration in the solution. CVs computed within the ER mechanism show significant discrepancies with the experimental ones ('early' GOR onset, no current peak), which leads us to conclude that the commonly accepted Fleischmann *et al.* [15] model is not entirely adequate to describe the electrooxidation of glucose on Ni.

A possible explanation for the current peak in the experimental CVs (Figure 2b) is glucose adsorption on $Ni(OH)_2$ active sites followed by reaction with NiOOH in a Langmuir-Hinshelwood reaction pathway [47]. Within this model both $Ni(OH)_2$ and NiOOH sites are required for the reaction to occur. Hence, the current drop at high potentials could be explained by the unavailability of the $Ni(OH)_2$ site for glucose adsorption at potentials significantly exceeding the standard potential of the $Ni(OH)_2$/NiOOH transition. To prove this, a LH kinetic model of the GOR, comprising of the steps 1, 5, 6, 7, was proposed.

$$Ni(OH)_2 + \text{glucose} \rightleftarrows Ni(OH)_2\text{–glucose}_{ads} \quad (5)$$

$$Ni(OH)_2\text{–glucose}_{ads} + NiOOH_{ads} \rightarrow Ni(OH)_2\text{– intermediate}_{ads} + Ni(OH)_2 \quad (6)$$

$$Ni(OH)_2\text{– intermediate}_{ads} + NiOOH_{ads} \rightarrow 2Ni(OH)_2 + \text{product} \quad (7)$$

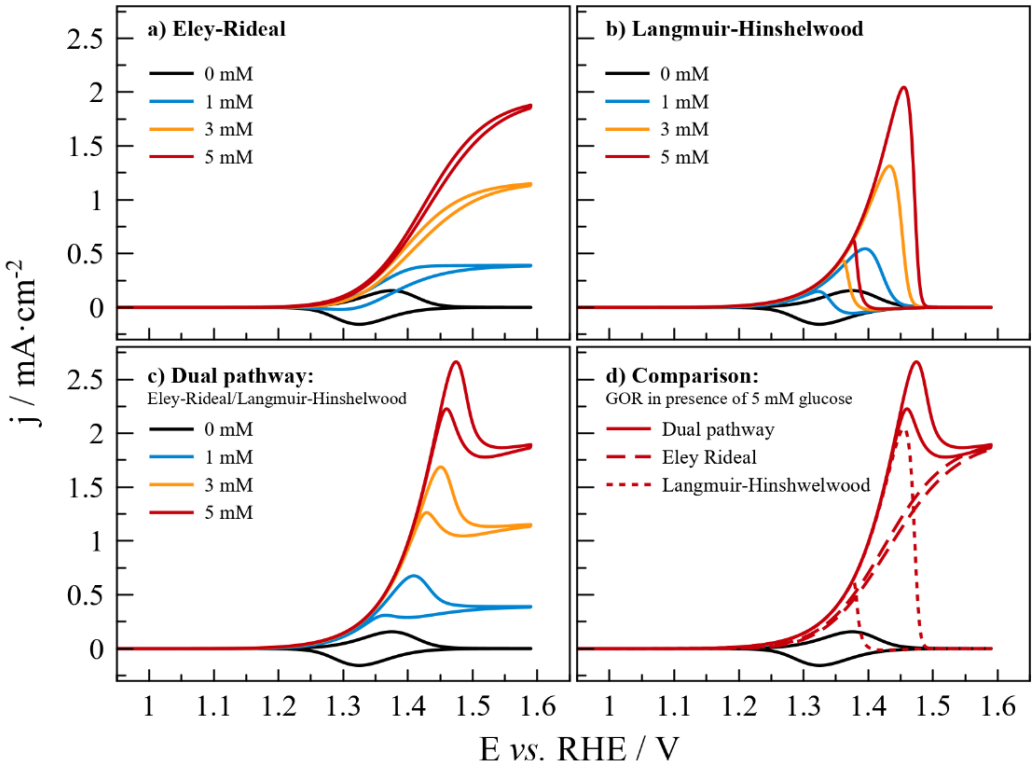

Figure 3. Cyclic voltammograms for the GOR on $Ni(OH)_2$/NiOOH at $\nu = 20$ mV·s^{-1} and different glucose concentrations simulated within various mechanisms: a) Eley-Rideal (ER), b) Langmuir-Hinshelwood (LH), c) a dual-path mechanism comprised of both an ER and a LH pathway, and d) comparison of different models for 5 mM glucose. Current density is given per unit of the geometric surface area. The parameters used for the simulations are given in Table S1.

Here glucose can reversibly absorb on $Ni(OH)_2$ active sites, and subsequently react with a NiOOH species to form the adsorbed intermediates. Finally the intermediate would react again with a NiOOH species to obtain the final product. The rates of the formation of $NiOOH_{ads}$, adsorbed glucose, adsorbed intermediate and product, as well as corresponding differential equations for the adsorbate coverages are specified in Supporting Information (S.4.4). The total Faradaic current density is then given by Eq. 8:

$$j_F = FS_t\left(k_1 \exp\left(\frac{\alpha F(E-E_1^\circ)}{RT}\right)(1-\theta_{NiOOH}-2\theta_{glucose}-2\theta_{int})-k_1\theta_{NiOOH}\exp\left(-\frac{(1-\alpha)F(E-E_1^\circ)}{RT}\right)\right) \quad (8)$$

Here $\theta_{glucose}$ is the coverage of adsorbed glucose on the surface, the meaning of the rest parameters is similar to the above. The CVs simulated using LH model are represented in Figure 3b, and as expected, exhibit current maximum, unlike in the ER model. The result corroborates glucose adsorption on the $Ni(OH)_2$ sites. However, one can also notice that, after surpassing the potential of the NiOOH formation, the current drops to zero, since, with the lack of the $Ni(OH)_2$ sites for glucose to adsorb, the reaction cannot proceed within

the LH mechanism. Such a behavior differs from the experimentally observed one (notably at glucose concentrations below 1 mM where a current plateau is observed), where the reaction does not drop to zero at high potentials.

Hence neither of the models presented above is capable to fully describe the GOR on Ni electrodes, albeit possessing certain characteristic features of the experimental system. For this reason, a dual-path mechanism comprised of an ER (steps 2' and 3') and a LH (steps 5 to 7) pathway was proposed in which both dissolved and adsorbed glucose can react with NiOOH. The rate constants for the formation of $NiOOH_{ads}$, $glucose_{ads}$, $intermediate_{ads}$ and product, as well as the corresponding differential equations for the adsorbate coverages are specified in Supporting Information (S.4.5). Total Faradaic current is again described by Equation 8, but surface coverages are now different due to the contributions of both the ER and LH pathways.

Figure 3c demonstrates the CVs simulated within the dual-path mechanism, which now semi-quantitatively reproduce the main characteristic features of the experimental data, namely the maximum current (due to the LH kinetics) and the sustained GOR current at high potential (attributed to the ER kinetics). The model assumes electrochemical NiOOH formation and its chemical reaction with glucose either arriving to the electrode surface from the bulk of the electrolyte, or adsorbed on the $Ni(OH)_2$ surface. The influence of potential scan rate on the CV simulated with the dual-path model in 1 mM glucose solution is shown in Figure S9. The simulations are in good agreement with the experimental data and can reproduce the experimentally observed overshadowing of the GOR at fast scan rate. However, even if the model captures the most important features of the experimental data, the low onset potential of the GOR could not be fully reproduced. Note that the 'onset' potential can be shifted towards lower potentials by varying rate constants k_3, k_{ads}, k_{des}, and k_4, as shown in Supporting Information (Figure S10 and Table S2) albeit not as much as observed in the experiment. An early onset could be explained by the presence of defects on the surface of electrodeposited Ni particles, where the NiOOH formation occurs at lower potentials than on a 'flat' surface. Such an assumption is supported by some previous studies performed with *in situ* Raman spectroscopy [31,38,43,48]. Furthermore, the differences in the shape of simulated and experimental CVs may be due to the formation of different surface phases (α/β-$Ni(OH)_2$, γ/β-NiOOH phases), 3D growth of the NiOOH layer, as well as formation of various reaction products.

3.4. Spectroelectrochemical measurements

Finally, *in situ* FTIRS measurements were performed on a Ni disk electrode to identify possible products of the GOR. The CVs of the Ni disk electrode in presence and absence of glucose in the FTIRS setup are shown in Figure S11, and exhibit similar characteristic features as the Ni_{ED}/GC electrode. Figure 4a shows

FTIR spectra obtained at different potentials applied in the presence of glucose. Since the spectra are presented after the background subtraction, the positive-pointing and negative-pointing absorption peaks correspond to the species whose concentration decreases and increases with time, respectively. Importantly, one can notice the appearance of several bands at 1350, 1385, 1583, 2732 and 2816 cm^{-1} at potentials as low as 1.17 V *vs.* RHE. Above 1.47 V *vs.* RHE (i.e. after the peak potential of the $Ni(OH)_2$/NiOOH transition), another vibration can be observed around 1417 cm^{-1}, suggesting changes in the mechanism of the GOR. Note that the spectra obtained at different times (Figure S12) clearly show that only the first product is initially observed even at the highest potential. To attribute the experimentally observed spectra to certain GOR products we turn to previous studies of the GOR by *in situ* FTIRS. For example *in situ* FTIRS investigation of the GOR on Au nanoparticles supported on carbon (AuNPs/C), $Au_{60}Pt_{40}$/C, and Pt_9Bi_1/C electrodes showed the formation of gluconate as the main product, which was also confirmed with HPLC measurements [49–51]. In those works, the presence of gluconate was corroborated by the appearance of the vibrations around 1580 and 1410 cm^{-1} (corresponding to the asymmetric and symmetric stretching of the carboxylate group, $\nu_{asym/sym}$ O-C-O), and 1350 cm^{-1} (corresponding to the bending of the methylene group, δ CH_2). Note that to the best of our knowledge no *in situ* FTIRS studies have been previously published for Ni electrodes.

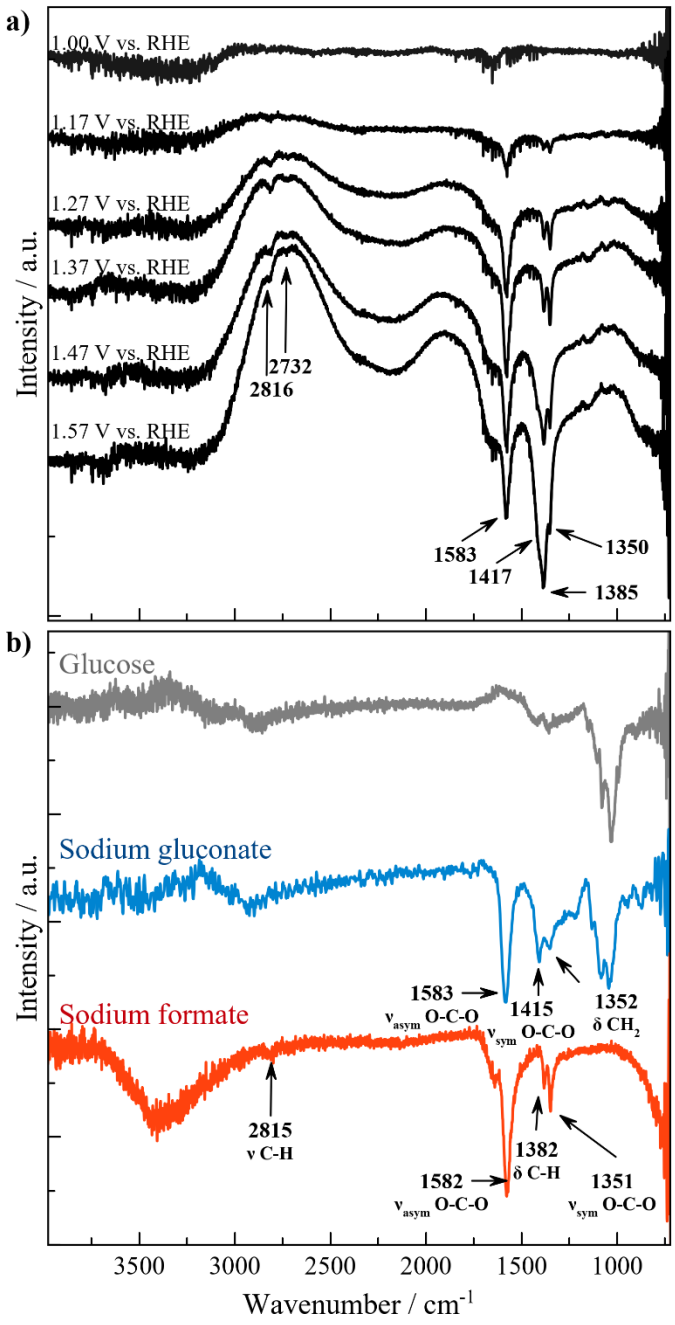

Figure 4. a) FTIR spectra recorded at different potentials in 0.1 M NaOH with 5 mM glucose at 25 °C with a Ni disk electrode, and b) FTIR spectra acquired in ATR configuration for solutions of 2 M glucose, 2 M sodium gluconate and 2 M sodium formate in 0.1 M NaOH. The FTIR spectra evolution with time is displayed in Figure S12 for each potential.

To help the assignment, FTIR spectra of reference glucose and gluconate were acquired in ATR configuration (Figure 4b). Both molecules present bands in the 1000 to 1250 cm^{-1} region, which originate from intramolecular vibrations, such as the CH_2OH group deformation, carbon ring deformation, C-H bond

bending, and C-H bond wagging [52]. In the case of gluconate, one may also observe characteristic bands at 1352, 1415 and 1583 cm^{-1} that are discussed in literature. However, while the 1352 and 1583 cm^{-1} vibrational bands corresponding to ν_{asym} and δ CH_2 vibration modes could be observed in our *in situ* FTIR spectra of Ni starting from 1.17 V vs. RHE, the O-C-O ν_{sym} at 1415 cm^{-1} characteristic of gluconate could only be observed at potential above 1.47 V vs. RHE. On other hand, the experimental spectra show very intense and unidentified bands at 1385 and 2816 cm^{-1}, which appear from the very beginning (Figures 4 and S12). We infer that the observed vibrational bands reflect formation of formate and can be attributed to δ CH [53] and ν C-H modes [54,55] respectively, the conclusion being corroborated by the reference spectrum of sodium formate shown in Figure 4b. Thus the above analysis suggests that formate is the main glucose oxidation product on $Ni(OH)_2$/NiOOH electrode at potentials lower than 1.47 V, while gluconate is only formed at higher potentials (and likely delayed in time), unlike what was previously assumed in several works [10,39,56,57]. Meanwhile, we need to admit that the identification of the possible products only from the FTIRS measurements is hardly possible and the presence of other compounds cannot be fully excluded. Online HPLC measurements are currently in progress and will complement the analysis.

4. Conclusions

$Ni(OH)_2$/NiOOH electrodes were prepared by electrodeposition of Ni on a glassy carbon substrate followed by electrochemical oxidation at high potential in 0.1 M NaOH electrolyte, and further used to study the electrooxidation of glucose in alkaline media. Measurements performed in Fe-purified and unpurified NaOH solutions showed significant difference in the CV shape, originating from the Fe-dependent contribution of the parasitic OER, but likely also from different contributions of various reaction pathways. A microkinetic model was developed to better understand the GOR pathways (Langmuir-Hinshelwood vs. Eley-Rideal) and the nature of the active sites ($Ni(OH)_2$ vs. NiOOH) on Ni. We conclude that both $Ni(OH)_2$ and NiOOH sites are needed for the GOR to occur, the $Ni(OH)_2$ required for the glucose adsorption, while the NiOOH sites – for its oxidation in a chemical step. We further infer that along with the Langmuir-Hinshelwood pathway involving adsorbed glucose and surface NiOOH species, an Eley-Rideal pathway is operating and involves NiOOH surface species reacting with glucose from solution, hence the GOR on Ni occurs in a dual-path mechanism. Finally, by employing operando FTIRS, we conclude that unlike previously believed, gluconate on $Ni(OH)_2$/NiOOH electrode is only formed at potentials above ~1.47 V vs. RHE, formate being the main glucose oxidation product at lower potentials.

Acknowledgements

This study was funded by the French National Research Agency (ANR): grant ANR-20-CE43-0005. Special thanks to Thierry Dintzer and Anne Boos for their help with SEM images and ICP-MS measurements.

CRediT author statement

Alejandra Medrano-Banda: Investigation, Visualization, Writing – original draft, Writing – review & editing. Julie Guehl: Investigation. Gwénaëlle Kéranguéven: Supervision, Writing – review & editing. Alexandr Oschepkov: Investigation, Methodology, Writing – review & editing. Antoine Bonnefont: Investigation, Conceptualization, Supervision, Writing – review & editing. Elena Savinova: Conceptualization, Supervision, Funding acquisition, Writing – review & editing.

References

[1] G.W. Huber, S. Iborra, A. Corma, Synthesis of transportation fuels from biomass: Chemistry, catalysts, and engineering, Chem Rev. 106 (2006) 4044–4098. https://doi.org/10.1021/cr068360d.

[2] A. Corma Canos, S. Iborra, A. Velty, Chemical routes for the transformation of biomass into chemicals, Chem Rev. 107 (2007) 2411–2502. https://doi.org/10.1021/cr050989d.

[3] D.S.P. Cardoso, B. Šljukić, D.M.F. Santos, C.A.C. Sequeira, Organic Electrosynthesis: From Laboratorial Practice to Industrial Applications, Org Process Res Dev. 21 (2017) 1213–1226. https://doi.org/10.1021/acs.oprd.7b00004.

[4] S. Kerzenmacher, J. Ducrée, R. Zengerle, F. von Stetten, Energy harvesting by implantable abiotically catalyzed glucose fuel cells, J Power Sources. 182 (2008) 1–17. https://doi.org/10.1016/j.jpowsour.2008.03.031.

[5] N. Neha, B.S.R. Kouamé, T. Rafaïdeen, S. Baranton, C. Coutanceau, Remarkably Efficient Carbon-Supported Nanostructured Platinum-Bismuth Catalysts for the Selective Electrooxidation of Glucose and Methyl-Glucoside, Electrocatalysis. 12 (2021) 1–14. https://doi.org/10.1007/s12678-020-00586-y.

[6] A. Brouzgou, P. Tsiakaras, Electrocatalysts for Glucose Electrooxidation Reaction: A Review, Top Catal. 58 (2015) 1311–1327. https://doi.org/10.1007/s11244-015-0499-1.

[7] C.C. Hu, T.C. Wen, Voltammetric investigation of palladium oxides-II. Their formation/reduction behaviour during glucose oxidation in NaOH, Electrochim Acta. 39 (1994) 2763–2771. https://doi.org/10.1016/0013-4686(94)00291-6.

[8] J. Hu, H. Lu, M. Li, G. Xiao, M. Li, X. Xiang, Z. Lu, Y. Qiao, Cobalt valence modulating in CoO incorporated carbon nanofiber for enhanced glucose electrooxidation, Materials Reports: Energy. 2 (2022) 100091. https://doi.org/10.1016/j.matre.2022.100091.

[9] J.T.C. Barragan, S. Kogikoski, E.T.S.G. Da Silva, L.T. Kubota, Insight into the Electro-Oxidation Mechanism of Glucose and Other Carbohydrates by CuO-Based Electrodes, Anal Chem. 90 (2018) 3357–3365. https://doi.org/10.1021/acs.analchem.7b04963.

[10] S.J. Li, W. Guo, B.Q. Yuan, D.J. Zhang, Z.Q. Feng, J.M. Du, Assembly of ultrathin NiOOH nanosheets on electrochemically pretreated glassy carbon electrode for electrocatalytic oxidation of glucose and methanol, Sens Actuators B Chem. 240 (2017) 398–407. https://doi.org/10.1016/j.snb.2016.09.002.

[11] D.E. Pissinis, L.E. Sereno, J.M. Marioli, Characterization of glucose electro-oxidation at Ni and Ni-Cr alloy electrodes, J. Electroanal. Chem. 694 (2013) 23–29. https://doi.org/10.1016/j.jelechem.2013.01.040.

[12] C. Xu, Y. Hu, J. Rong, S.P. Jiang, Y. Liu, Ni hollow spheres as catalysts for methanol and ethanol electrooxidation, Electrochem. Commun. 9 (2007) 2009–2012. https://doi.org/10.1016/j.elecom.2007.05.028.

[13] Q. Lin, Y. Wei, W. Liu, Y. Yu, J. Hu, Electrocatalytic oxidation of ethylene glycol and glycerol on nickel ion implanted-modified indium tin oxide electrode, Int J Hydrogen Energy. 42 (2017) 1403–1411. https://doi.org/10.1016/j.ijhydene.2016.10.011.

[14] S. Lu, M. Hummel, Z. Gu, Y. Wang, K. Wang, R. Pathak, Y. Zhou, H. Jia, X. Qi, X. Zhao, B. Bin Xu, X. Liu, Highly Efficient Urea Oxidation via Nesting Nano-Nickel Oxide in Eggshell Membrane-Derived Carbon, ACS Sustain Chem Eng. 9 (2021) 1703–1713. https://doi.org/10.1021/acssuschemeng.0c07614.

[15] M. Fleischmann, K. Korinek, D. Pletcher, THE OXIDATION OF ORGANIC COMPOUNDS AT A NICKEL ANODE IN ALKALINE SOLUTION, n.d.

[16] A.J. Bard, L.R. Faulkner, Electrochemical methods : fundamentals and applications, n.d.

[17] D.D. Macdonald, J. Anderson, Transient Techniques in Electrochemistry, 1979. https://doi.org/10.1149/1.2128855.

[18] I. Danaee, M. Jafarian, F. Forouzandeh, F. Gobal, M.G. Mahjani, Impedance spectroscopy analysis of glucose electro-oxidation on Ni-modified glassy carbon electrode, Electrochim. Acta. 53 (2008) 6602–6609. https://doi.org/10.1016/j.electacta.2008.04.042.

[19] I. Danaee, M. Jafarian, F. Forouzandeh, F. Gobal, M.G. Mahjani, Kinetic interpretation of a negative time constant impedance of glucose electrooxidation, J. Phys. Chem. B. 112 (2008) 15933–15940. https://doi.org/10.1021/jp8069173.

[20] I. Danaee, M. Jafarian, F. Forouzandeh, F. Gobal, Kinetic studies of glucose electrocatalytic oxidation on GC/Ni electrode, Int. J. Chem. Kinet. 44 (2012) 712–721. https://doi.org/10.1002/kin.20721.

[21] M.T. Bender, Y.C. Lam, S. Hammes-Schiffer, K.S. Choi, Unraveling Two Pathways for Electrochemical Alcohol and Aldehyde Oxidation on NiOOH, J. Am. Chem. Soc. 142 (2020) 21538–21547. https://doi.org/10.1021/jacs.0c10924.

[22] K.E. Toghill, L. Xiao, M.A. Phillips, R.G. Compton, The non-enzymatic determination of glucose using an electrolytically fabricated nickel microparticle modified boron-doped diamond electrode

or nickel foil electrode, Sens. Actuator. B-Chem. 147 (2010) 642–652. https://doi.org/10.1016/j.snb.2010.03.091.

[23] C. Zhao, C. Shao, M. Li, K. Jiao, Flow-injection analysis of glucose without enzyme based on electrocatalytic oxidation of glucose at a nickel electrode, Talanta. 71 (2007) 1769–1773. https://doi.org/10.1016/j.talanta.2006.08.013.

[24] G. Młynarek, M. Paszkiewicz, A. Radniecka, The effect of ferric ions on the behaviour of a nickelous hydroxide electrode, J. Appl. Electrochem. 14 (1984) 145–149. https://doi.org/10.1007/BF00618733.

[25] D.A. Corrigan, The Catalysis of the Oxygen Evolution Reaction by Iron Impurities in Thin Film Nickel Oxide Electrodes, J. Electrochem. Soc. 134 (1987) 377–384. https://doi.org/10.1149/1.2100463.

[26] S. Anantharaj, S. Kundu, S. Noda, "The Fe Effect": A review unveiling the critical roles of Fe in enhancing OER activity of Ni and Co based catalysts, Nano Energy. 80 (2021) 105514. https://doi.org/10.1016/j.nanoen.2020.105514.

[27] C. Xiang, Q. Xie, S. Yao, Electrochemical Quartz Crystal Impedance Study of Glucose Oxidation on a Nickel Hydroxide Modified Au Electrode in Alkaline Solution, Electroanalysis 15 (2003) 987-990. https://doi.org/10.1002/elan.200390120

[28] A.G. Oshchepkov, G. Braesch, A. Bonnefont, E.R. Savinova, M. Chatenet, Recent Advances in the Understanding of Nickel-Based Catalysts for the Oxidation of Hydrogen-Containing Fuels in Alkaline Media, ACS Catal. 10 (2020) 7043–7068. https://doi.org/10.1021/acscatal.0c00101.

[29] R.A. Márquez, K. Kawashima, Y.J. Son, G. Castelino, N. Miller, L.A. Smith, C.E. Chukwuneke, C.B. Mullins, Getting the Basics Right: Preparing Alkaline Electrolytes for Electrochemical Applications, ACS Energy Lett. 8 (2023) 1141–1146. https://doi.org/10.1021/acsenergylett.2c02847.

[30] V.M. Zemtsova, A.G. Oshchepkov, E.R. Savinova, Unveiling the Role of Iron in the Nickel-Catalyzed Urea Oxidation Reaction, ACS Catal. (2023) 13466–13473. https://doi.org/10.1021/acscatal.3c03126.

[31] S. Klaus, Y. Cai, M.W. Louie, L. Trotochaud, A.T. Bell, Effects of Fe electrolyte impurities on $Ni(OH)_2$/NiOOH structure and oxygen evolution activity, J. Phys. Chem. C. 119 (2015) 7243–7254. https://doi.org/10.1021/acs.jpcc.5b00105.

[32] B. Beden, D.J.M.L. Floner, C. Lamy, A VOLTAMMETRIC STUDY OF THE FORMATION OF HYDROXIDES AND OXYHYDROXIDES ON NICKEL SINGLE CRYSTAL ELECTRODES IN CONTACT WITH AN ALKALINE SOLUTION, Surface Science 162 (1985) 822-829. https://doi.org/10.1016/0039-6028(85)90985-9

[33] A.G. Oshchepkov, G. Braesch, G. Rostamikia, A. Bonnefont, M.J. Janik, M. Chatenet, E.R. Savinova, Insights into the borohydride electrooxidation reaction on metallic nickel from operando FTIRS, on-line DEMS and DFT, Electrochim. Acta. 389 (2021). https://doi.org/10.1016/j.electacta.2021.138721.

[34] E.A. Vorms, E.A. Suprun, A. V. Nartova, R.I. Kvon, A.G. Oshchepkov, Electrodeposited NiCu nanoparticles for the borohydride oxidation reaction: Effect of Cu on the activity and stability of Ni

upon surface oxidation, Electrochim. Acta. 433 (2022). https://doi.org/10.1016/j.electacta.2022.141196.

[35] D.S. Hall, C. Bock, B.R. MacDougall, The Electrochemistry of Metallic Nickel: Oxides, Hydroxides, Hydrides and Alkaline Hydrogen Evolution, J. Electrochem. Soc. 160 (2013) F235–F243. https://doi.org/10.1149/2.026303jes.

[36] M. Kim, K. Kim, A Study on the Phase Transformation of Electrochemically Precipitated Nickel Hydroxides Using an Electrochemical Quartz Crystal Microbalance, J. Electrochem. Soc. 145 (1998) 507–511. https://doi.org/10.1149/1.1838294/XML.

[37] W. Sheng, M. Myint, J.G. Chen, Y. Yan, Correlating the hydrogen evolution reaction activity in alkaline electrolytes with the hydrogen binding energy on monometallic surfaces, Energy Environ. Sci. 6 (2013) 1509–1512. https://doi.org/10.1039/C3EE00045A.

[38] D. Friebel, M.W. Louie, M. Bajdich, K.E. Sanwald, Y. Cai, A.M. Wise, M.J. Cheng, D. Sokaras, T.C. Weng, R. Alonso-Mori, R.C. Davis, J.R. Bargar, J.K. Nørskov, A. Nilsson, A.T. Bell, Identification of highly active Fe sites in (Ni,Fe)OOH for electrocatalytic water splitting, J. Am. Chem. Soc. 137 (2015) 1305–1313. https://doi.org/10.1021/ja511559d.

[39] K.E. Toghill, R.G. Compton, Electrochemical Non-Enzymatic Glucose Sensors: A Perspective and an Evaluation, Int. J. Electrochem. Sci. 5 (2010) 1246 - 1301.

[40] Q. Yi, W. Huang, W. Yu, L. Li, X. Liu, Hydrothermal synthesis of titanium-supported nickel nanoflakes for electrochemical oxidation of glucose, Electroanalysis. 20 (2008) 2016–2022. https://doi.org/10.1002/elan.200804282.

[41] I.-H. Yeo, D.C. Johnson, Electrochemical response of small organic molecules at nickel-copper alloy electrodes, , J. Electroanal. Chem. 495 (2001) 110-119. https://doi.org/10.1016/S0022-0728(00)00401-0

[42] A.G. Oshchepkov, A. Bonnefont, V.A. Saveleva, V. Papaefthimiou, S. Zafeiratos, S.N. Pronkin, V.N. Parmon, E.R. Savinova, Exploring the Influence of the Nickel Oxide Species on the Kinetics of Hydrogen Electrode Reactions in Alkaline Media, Top Catal. 59 (2016) 1319–1331. https://doi.org/10.1007/s11244-016-0657-0.

[43] M.W. Louie, A.T. Bell, An investigation of thin-film Ni-Fe oxide catalysts for the electrochemical evolution of oxygen, J. Am. Chem. Soc. 135 (2013) 12329–12337. https://doi.org/10.1021/ja405351s.

[44] A. de G. P. Oliva, J. Leonardi, J.F. Laurent, C. Delmas, J.J. Braconnier, M. Figlarz, F. Fievet, Review of the structure and the electrochemistry of nickel hydroxides and oxy-hydroxides, J. Power Sources. 8 (1982) 229–255. https://doi.org/10.1016/0378-7753(82)80057-8.

[45] I. Chorkendorff, J.W. Niemantsverdriet, Concepts of Modern Catalysis and Kinetics, Wiley-VCH, 2003.

[46] D.D. Eley, E.K. Rideal, Parahydrogen conversion on tungsten, Nature. 146 (1940) 401–402. https://doi.org/10.1038/146401d0.

[47] C.J. Danby, J.G. Davoud, D.H. Everett, C.N. Hinshelwood, R.M. Lodge, The Kinetics of Absorption of Gases from an Air Stream by Granular Reagents, J. Chem. Soc. (1946) 918-934.. https://doi.org/10.1039/jr9460000918.

[48] B.S. Yeo, A.T. Bell, In Situ Raman Study of Nickel Oxide and Gold-Supported Nickel Oxide Catalysts for the Electrochemical Evolution of Oxygen, *Phys. Chem. C* 116 (2012) 8394–8400. https://doi.org/10.1021/jp3007415

[49] N. Neha, T. Rafaïdeen, T. Faverge, F. Maillard, M. Chatenet, C. Coutanceau, Revisited Mechanisms for Glucose Electrooxidation at Platinum and Gold Nanoparticles, Electrocatalysis. (2022). https://doi.org/10.1007/s12678-022-00774-y.

[50] A.H.B. Dourado, A.G.M. da Silva, F.A.C. Pastrián, R.L. Munhos, A.P. de Lima Batista, A.G.S. de Oliveira-Filho, J. Quiroz, D.C. de Oliveira, P.H.C. Camargo, S.I. Córdoba de Torresi, In situ FTIR insights into the electrooxidation mechanism of glucose as a function of the surface facets of Cu2O-based electrocatalytic sensors, J. Catal. 375 (2019) 95–103. https://doi.org/10.1016/j.jcat.2019.05.032.

[51] E.G. Mahoney, W. Sheng, M. Cheng, K.X. Lee, Y. Yan, J.G. Chen, Analyzing the electrooxidation of ethylene glycol and glucose over platinum-modified gold electrocatalysts in alkaline electrolyte using in-situ infrared spectroscopy, J. Power Sources. 305 (2016) 89–96. https://doi.org/10.1016/j.jpowsour.2015.11.059.

[52] C. Song, W.H. Fan, L. Ding, X. Chen, Z.Y. Chen, K. Wang, Terahertz and infrared characteristic absorption spectra of aqueous glucose and fructose solutions, Sci. Rep. 8 (2018). https://doi.org/10.1038/s41598-018-27310-7.

[53] S.C. Chang, Y. Ho, M.J. Weaver, Applications of Real-Time FTIR Spectroscopy to the Elucidation of Complex Electroorganic Pathways: Electrooxidation of Ethylene Glycol on Gold, Platinum, and Nickel in Alkaline Solution, J. Am. Chem. Soc. 113 (1991) 9506–9513. https://doi.org/10.1021/ja00025a014.

[54] G. Lucazeau, C. Sandorfy, The near-infrared spectra of some simple aldehydes, Can. J. Chem. 48 (1970) 3694–3703. https://doi.org/10.1139/v70-618.

[55] K. Ito, H.J. Bernstein, the Vibrational Spectra of the Formate, Acetate, and Oxalate Ions, Can. J. Chem. 34 (1956) 170–178. https://doi.org/10.1139/v56-021.

[56] A.M. Ghonim, B.E. El-Anadouli, M.M. Saleh, Electrocatalytic glucose oxidation on electrochemically oxidized glassy carbon modified with nickel oxide nanoparticles, Electrochim. Acta. 114 (2013) 713–719. https://doi.org/10.1016/j.electacta.2013.10.115.

[57] L. Shabnam, S.N. Faisal, A.K. Roy, V.G. Gomes, Nickel-Nanoparticles on Doped Graphene: A Highly Active Electrocatalyst for Alcohol and Carbohydrate Electrooxidation for Energy Production, ChemElectroChem. 5 (2018) 3799–3808. https://doi.org/10.1002/celc.201800818.